Keysight Technologies

DesignCon 2014
Modeling, Extraction and Verification of VCSEL Model for Optical IBIS AMI

White Paper

KEYSIGHT TECHNOLOGIES

Abstract

A technique of modeling and extraction of VCSEL devices for IBIS-AMI has been proposed. With the measured L-I and V-I curves of the VCSEL, a behavior model is extracted from rate-equation model that includes thermal effects. Here two suitable curve fitting algorithms are used. This model exhibits the observed performance in both time and frequency domains. It has been verified on several mainstream VCSEL devices where a consistent fitting between the measured data and abstracted one is achieved. And the results prove that the modeling, extraction and verification process can abstract a real VCSEL device accurately. The generation of an IBIS-AMI model facilitates system designs that include VCSEL devices. Also a certain VCSEL can be published into a dynamic link library. This technique is intended to help VCSEL vendors build and publish behavior models with the measured device characteristics. By following the IBIS-AMI standard, VCSEL users can simulate their designs more conveniently.

Authors'

Zhaokai Yuan, Keysight Technologies, Inc.
M. V. Ramana Murty, Avago Technologies, Inc.
Sanjeev Gupta, Avago Technologies, Inc.
Amolak Badesha, Avago Technologies, Inc.

Authors Biographies

Zhaokai Yuan is at Keysight Technologies EEsof division as a R&D system engineer of the SystemVue team. He mainly focuses on Wireless Communication libraries and High Speed Digital libraries developing.

Ramana Murty joined the Fiber Optics III-V Division at Avago Technologies in 2007. He led the development of 850 nm 10G VCSELs for high performance computing and 100 GbE applications. His current interests include the development of VCSELs and p-i-n photodetectors for 25G applications.

Sanjeev Gupta is currently employed by Avago Technology Fiber Optic division as Sr. R&D Manager and is leading a team of Signal Integrity, EMI and Layout engineers. From 1994 to 2011 he was employed by Keysight Technologies and held various application engineering positions. He has co-authored numerous papers and was recipient of DesignCon best paper award consecutively for three years (2008, 2009 and 2010).

Amolak Badesha is Program Director at Avago Technologies, driving strategic initiatives championed by executive management at Fiber Optics Division. Previously, Amolak built and lead the SI/EMI team at Avago's Fiber Optic Division. Amolak also spent 7 years at Keysight's EEsof Division, specializing in high-speed design. While at Keysight, Amolak made key contributions to innovative products like Automated AMI model generation and Optical AMI modeling.

I Introduction

The transceiver market has been growing rapidly over the past few years due to the increasing demand of large-scale data communications. An optical link is an effective solution because of high bandwidth and low power consumption.

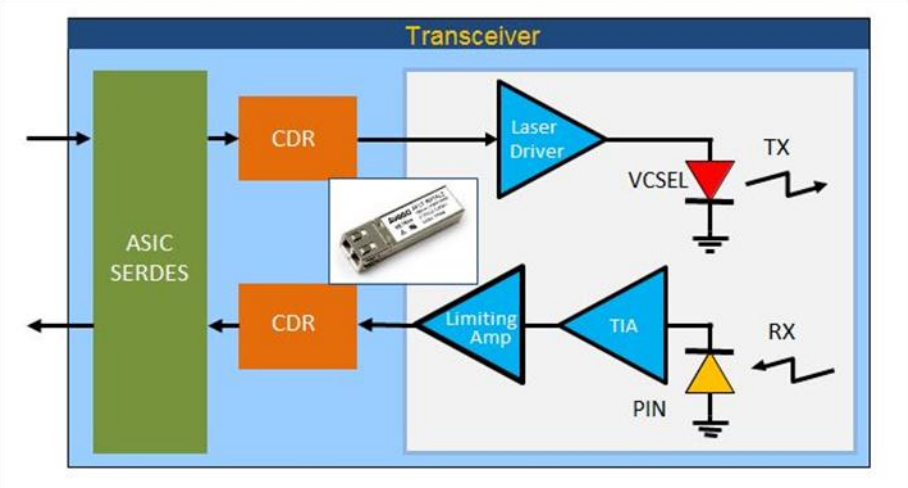

Figure 1 Block Diagram of an Optical Link

As illustrated in Figure 1, an optical link consists of Laser Driver, Vertical cavity surface emitting laser (VCSEL), Photo-detector, trans-impedance amplifier (TIA), Limiting Amplifier, optical fiber and clock-data-recovery (CDR). The electrical signal is received from the host board through pluggable or embedded optical module. The received signal goes through signal conditioning to improve signal quality in terms of its amplitude and timing before it is converted to an optical signal. Electrical receiver on the Optical transmitter can utilize various equalization schemes such as Continuous Time Equalizer or De-emphasis before the signal jitter performance is improved using clock and data recovery circuit. Laser driver following receives the signal from CDR output and convert it into a current waveform which drives VCSEL diode. For short range communication, VCSEL provides many advantages such as low power requirements and low cost over other types of electro-optics devices such as DFBs. The output signal from the VCSEL is coupled to a multimode optical fiber using precision optical techniques. On the receiver end, High speed optical signal is received by the p-i-n photo-detector which converts incoming light to a current waveform. The TIA following the p-i-n diode transforms the current waveform into an output voltage waveform. The signal passes through limiting amplifier stages before this data is re-timed and equalized to the host receiver.

In this data link, VCSEL is a key device due to its unique electro-optic characteristics [1] [2] [3]and it is important to model the VCSEL to simulate the performance of an integrated data communication system. Here, a first principles model [4] of a VCSEL is not required. An effective theory in the form of rate equations captures the behavior of the VCSEL [5] [6] [7] [8].

The paper is organized as follows. A rate equation model for the VCSEL including thermal effects is described in section II and the method extracting the model

parameters is described in section III. The VCSEL model is applied to three devices from literature in section IV followed by a conclusion.

II VCSEL Modeling and Parameter Extraction

Rate Equation Based Thermal VCSEL Model

The VCSEL device characteristics can be described by a set of coupled of non-linear rate equations. While the rate equations are traditionally expressed in terms of carrier and photon densities, here we use the carrier N and photon S numbers. Electrons and holes (here represented by N) are injected into the active region of the VCSEL by an applied voltage across the junction, and lost through stimulated emission and other (spontaneous emission and non-radiative) paths. The non-radiative and spontaneous emission paths are captured through a carrier lifetime τ_n in the rate equation. Photons are generated by stimulated and spontaneous emission, and lost through the partially transparent mirrors and other (absorption, scattering) optical losses. The total optical loss is captured through a photon lifetime τ_p. Stimulated emission depends on the gain in the active region and is a function of carrier density and a (weak) function of photon density. The rate equations can be descripted as Equation 1 and Equation 2.

$$\frac{dN}{dt} = \frac{\eta_i (I - I_{off}(T))}{q} - \frac{N}{\tau_n} - \frac{G_o (N - N_o) S}{1 + \varepsilon S} \qquad \textbf{Equation 1}$$

$$\frac{dS}{dt} = -\frac{S}{\tau_p} + \frac{\beta N}{\tau_n} + \frac{G_o (N - N_o) S}{1 + \varepsilon S} \qquad \textbf{Equation 2}$$

where η_i is the carrier injection efficiency, G_0 is the gain coefficient, N_0 is the carrier transparency number, β is the spontaneous emission factor, ε is the gain compression factor, and q is the electron charge. The drive current is I and $I_{off}(T)$ is a temperature dependent offset current described below. Certain simplifications have been made in the description of the VCSEL and are duly noted. Most VCSELs used in practical applications are multi-mode with significant photon populations in several transverse modes. They are more accurately represented by a rate equation for the photon number S_1, S_2, … in each transverse mode. Here, a single photon number $S = S_1 + S_2 + \ldots$ is used to capture the behavior of the device. The active region gain has been approximated as a linear function of N. Finally, carrier transport effects have been ignored [7].

Light emitted P_0 from the VCSEL is proportional to the photon density

$$P_o = kS \qquad \textbf{Equation 3}$$

and can also be expressed in terms of the drive current

$$P_o = \eta (I - I_{tho} - I_{off}(T)) \qquad \textbf{Equation 4}$$

Here *k* is a scale-factor that includes the output coupling efficiency through the distributed Bragg mirror in the VCSEL, the photon energy and the photon lifetime [7]. The parameter η represents the slope efficiency, and I_{th0} is the threshold current at a reference temperature. Light emitted by a VCSEL is a function of temperature and this is incorporated through the $I_{off}(T)$ term. An empirical expression is used for the offset current

$$I_{off} = \sum_{k=0}^{M} a_k T^k \qquad \textbf{Equation 5}$$

A polynomial of order M = 4 is found to provide an adequate description. It is noted that the temperature variation of both slope efficiency and threshold current of a VCSEL is captured by the $I_{off}(T)$ term.

The junction temperature T can be related to the ambient temperature T_0 and the input electrical power by

$$T = T_o + (IV - P_o)R_{th} - \tau_{th}\frac{dT}{dt} \qquad \textbf{Equation 6}$$

where V is the applied voltage and R_{th} is the device thermal resistance. The last term with the time constant τ_{th} represents a reactive load. It vanishes under dc conditions. Also, junction temperature does not change significantly during high data rate (> 1 Gb/s) modulation. With increasing drive current, the junction temperature T increases causing $I_{off}(T)$ term to increase. Eventually, at a certain drive current $\Delta I = \Delta I_{off}(T)$ and the light emitted does not increase any further. This is the rollover current and a further increase in drive current causes P_0 to decrease.

Calculation of the junction temperature requires knowledge of the applied voltage and this is achieved by modeling the IV characteristic of the VCSEL. Three different functions between V and I are proposed in [5], Equation 7, Equation 8 and Equation 9.

$$V = c_0 R_s + c_1 \ln(1 + \frac{I}{c_2}) \qquad \textbf{Equation 7}$$

$$V = \sum_{p=0}^{P} b_p I^p \cdot \sum_{q=0}^{Q} c_q T^q \qquad \textbf{Equation 8}$$

$$V = \sum_{p=0}^{P} b_p I^p \qquad \textbf{Equation 9}$$

Equation 7 describes a resistance in series with a diode. Equation 8 treats the voltage as a polynomial function of current and temperature. Equation 9 is a reduced version of Equation 8 where the impact of temperature has been ignored.

The VCSEL can be modeled and simulated using the equations described above. The non-linear nature of the equations requires the development of a curve fitting algorithm for extraction of the parameters.

Curve Fitting Algorithms

Two curve fitting algorithms have been used to fit the experimentally measured device characteristics. The first is the linear least squares method, and the second is the non-linear least squares method for equations that involve products of quantities.

Linear Least Squares Curve Fitting

The linear least squares curve fitting algorithm is used to extract the coefficients in polynomial equations such as the relationship between the offset current and the temperature, and between laser voltage and current. Consider a polynomial function f describing the relationship between x and y

$$y = f(x) = \sum_{k=0}^{L} a_k x^k \quad \textbf{Equation 10}$$

The goal is to extract the optimum values of coefficients a_k from a data set $(x_1, y_1), (x_2, y_2) \ldots, (x_n, y_n)$. The optimum values are obtained by minimizing the sum of squares [5]:

$$\Pi = \sum_{i=1}^{n} [y_i - f(x_i)]^2 \quad \textbf{Equation 11}$$

The result is a system of L simultaneous linear equations in the coefficients $\{a_k\}$ that can be solved for the coefficients by standard linear algebra technique, e.g. LU decomposition of the coefficient matrix. Another approach is to use an orthonormal basis instead of the original basis. The orthonormal basis can be got by the Schmidt orthogonalization process, where an iteration process is taken instead which is more easily implemented on computer.

$$\begin{aligned} &P_0(x) = 1, \\ &P_1(x) = (x - \alpha_1) P_0(x) \\ &P_{k+1}(x) = (x - \alpha_{k+1}) P_0(x) - \beta_k P_{k-1}(x) \\ &(k = 0,1,\ldots, n-1) \end{aligned} \quad \textbf{Equation 12}$$

Where the $P_k(x)$ is a polynomial with the order of k, and

$$\alpha_{k+1} = \frac{\sum_{i=0}^{m} x_i P_k^2(x_i)}{\sum_{i=0}^{m} P_k^2(x_i)} = \frac{(xP_k, P_k)}{(P_k, P_k)}, \quad \beta_k = \frac{\sum_{i=0}^{m} P_k^2(x_i)}{\sum_{i=0}^{m} P_{k-1}^2(x_i)} = \frac{(P_k, P_k)}{(P_{k-1}, P_{k-1})}.$$

Non-Linear Least Squares Curve Fitting

The non-linear least squares curve fitting algorithm is used to extract parameter values from the more complex equations, such as the rate equations and the stationary LI model equations. Both the two kinds of equations cannot be solved directly and contain multiple

parameters. So a total different thought is taken compared to the Linear LS algorithm. The final solution is achieved by multiple trying. One or more measured data is used as a target item. For each loop, one possible set of parameter values are preset and then the target item is calculated with the equations. The differences are collected together and multiplied with the according weight separately. And this is the error of current set of parameter values. During the multiple try, the minimal error can be got and the corresponding set of parameter values is taken as the final solution. In this algorithm, the chosen of possible values are very important. A reasonable range of the being extracted variable should be a precondition. Within the rage, a random value generation method is taken that is how the certain set of value is chosen out. So the issue that how many values are selected exists in this method. If the number is too small, the best value cannot be picked out correctly. And if more details are considered, the calculation will cost too much time. To resolve this issue, an iteration process is brought in. The range is reduced gradually along with the increasing of iteration number.

III VCSEL Parameter Extraction

The procedure for extracting the various coefficients from measured VCSEL characteristics is described in this subsection. Commonly measured characteristics of a VCSEL include the LI, VI and small-signal modulation response S_{21}. Measurement at multiple temperatures provides a more complete data set for generating the VCSEL model.

Coefficients in the LI Curve

A typical LI curve shows a threshold current for lasing, a linear increase in output power P_0 for small currents above threshold current, and a rollover point beyond which P_0 decreases with increasing current. Equations 4 – 6 describe the LI curve and are collected here for reference.

$$\begin{cases} P_o = \eta(I - I_{tho} - I_{off}(T)) \\ T = T_o + (IV - P_o)R_{th} \\ I_{off} = \sum_{k=0}^{M} a_k T^k \end{cases}$$

As the LI curve is collected under dc condition, the term dT/dt in equation 6 vanishes. The thermal time constant τ_{th} for a VCSEL is on the order of 1 μs. Thus, fortunately, the dT/dt term can be ignored under both dc and multi-Gb/s modulation. The junction has adequate time to adjust to the drive current under dc condition whereas under multi-Gb/s modulation, the junction temperature does not have the time to adjust to the varying drive current (provided the series of 1's and 0's are short compared to τ_{th}). The non-linear least squares fitting method is used to extract the coefficients η, I_{tho}, R_{th}, and $\{a_k\}$ with M = 4.

Coefficients in the VI Curve

Three analytical models were proposed in Equation 7, Equation 8 and Equation 9 to model the VI curve. Equation 7 is further approximated by

$$V = c_0 + c_1 I + c_2 \log(I) \qquad \textbf{Equation 13}$$

to facilitate a linear least squares fitting method. The coefficients $\{c_i\}$ are then extracted from the measured VI curve. Similarly, the coefficients in Equation 9 can be obtained from a linear least squares fit. The effect of temperature is ignored in both Equation 9 and Equation 13.

Equation 8 takes temperature into account by using a polynomial expansion in both current and temperature. The temperature is calculated from equation 6 at each current using the thermal resistance R_{th} obtained by fitting the LI curve. Equation 8 can be expanded to

$$V = p_0 + p_{11} IT + p_{12} IT^2 + p_{21} I^2 T + \cdots + p_{ij} I^i T^j + \cdots + p_{PQ} I^P T^Q \qquad \textbf{Equation 14}$$

and the coefficients can be obtained from the linear least squares method. The total number of coefficients is PQ – 1.

Coefficients in the Rate Equations

The rate equations are expressed in terms of the carrier and photon numbers that are not measured experimentally. In steady state, the rate of change of carrier and photon number is zero resulting in

$$\frac{\eta_i (I - I_{off}(T))}{q} - \frac{N}{\tau_n} - \frac{G_o (N - N_o) S}{1 + \varepsilon S} = 0 \qquad \textbf{Equation 15}$$

$$-\frac{S}{\tau_p} + \frac{\beta N}{\tau_n} + \frac{G_o (N - N_o) S}{1 + \varepsilon S} = 0 \qquad \textbf{Equation 16}$$

By substituting the S with P_o and k in Equation 3 , combining with Equation 4 where the $I_{off}(T)$ can be instead and uniting the above two equations together, one equations only with the relation of the measured data (P_o, I and V) and the parameters (η_i, β, τ_n, τ_p, G_o, N_o, ε) is generated.

$$I_{cur} = \frac{q \cdot (G_o \beta P_o^2 / k^2 + (1 + G_o N_o \tau_p (1 - \beta) P_o) / k)}{\eta_i \tau_p (\beta + G_o \tau_n P_o / k)} + I_{tho} + I_{off} \qquad \textbf{Equation 17}$$

$$\begin{aligned} N_s &= P_o / (k \tau_p) + \frac{G_o N_o P_o / (k + \varepsilon P_o)}{\beta / \tau_n + G_o P_o / (k + \varepsilon P_o)} \\ S_s &= \frac{\eta_i (I - I_{off}) / q - N_s / \tau_n}{G_o (N_s - N_o)} \\ P_{od} &= k S_s \end{aligned} \qquad \textbf{Equation 18}$$

If the frequency response curve for the small modulated signal can be provided, the extraction can adopt this dynamic characteristic. An extraction method has been

introduced in [6] and [8], by some modification on the rate equations, the frequency response for the current rate equations can be descripted by Equation 19.

$$H(f) = \frac{Z}{(j2\pi \cdot f)^2 + j \cdot 2\pi \cdot f \cdot Y + Z} \qquad \textbf{Equation 19}$$

Where $Y = \frac{G_o P_o}{k + \varepsilon P_o} + \frac{1}{\tau_p} + \frac{1}{\tau_n} - \frac{G_o(N_s - N_o)}{(1 + \varepsilon P_o / k)^2}$ and $Z = \frac{G_o P_o}{(k + \varepsilon P_o)\tau_p} + \frac{(\beta - 1) G_o (N_s - N_o)}{(1 + \varepsilon P_o / k)^2 \tau_n} + \frac{1}{\tau_n \tau_p}$.

In this step, the non-linear curve fitting algorithm is applied. The final error consists of three parts. The first part comes from the stationary relationship that how much current is needed to convert the present light power. I_{cur} is the effect current for light conversion. Equation 17 uses it as the target. The measurement error is got from the comparison between the measured and the calculated. The second part comes from the dynamic calculation of light power. In this calculation, the light power is got from the multiplication of the scaling-factor and the number of photons. In Equation 18, N_s means the number of carriers for current stationary case. It is first calculated. By inserting the N_s into the second equation, the number of photons S_s can be got. Then the P_{od} can be easily got. The calculated P_{od} and the measured P_o contribute the second part of the final error. The last part comes from the fitting result of the frequency response curve. Equation 19 is used to get the calculated frequency response. By comparison with the measured ones, the last part of error is got. The three parts of errors are allocated with a pre-defined weight. The best parameter values are got when the minimal error is achieved.

Up to now, the parameter values are got. This is the set that can stand for the current VCSEL. The integration of the parameter values and the rate equations is the behavior model. The simulation of VCSEL is also based on the rate equations. With the extraction, the VCSEL is abstract successfully into a behavior model. By substituting the parameter into the specific value and calculating the rate equations step by step on time domain, the behavior of VCSEL is simulated.

IV VCSEL Model Verification

Device 1

The first device is an 863-nm VCSEL, as reported in [9]. The LI curves under the ambient temperature to be 20℃, 40℃, 60℃, 80℃, 100℃ and 120℃ are provided. The degree C is used to descript the temperature in this paper. Also the room-temperature VI curve is provided. In this extraction, we choose the Equation 9 to extract the VI curve. The LI and VI curves fitting result is shown in Figure 2. And the abstract behavior model has the value of η =0.399619, R_{th} =2.80217℃/mW, I_{tho} =0.306942mA, the coefficients to calculate offset $\{a_0, a_1, a_2, a_3, a_4\}$= {1.35978mA, 0.439447e-2mA/K, 0.788546e-4mA/K^2, 0.353605e-6mA/K^3, 0.00607852e-8mA/K^4}, η_i = 0.623601, β =1.00003e-7, τ_n =5.29655ns, k =4.16084e-8W, G_o =8.5398e5, N_o =1.84006e6, τ_p =2.47ps, ε =1.72085e-

17. As the VI curve is fitted by the LS algorithm, an orthogonal base is used. The coefficients array and the related auxiliary array (α and β) are {3.39,34.07,-1.31e3,6.22e4,-2.72e6,8.33e7,5.36e9}, {0,0.0219,0.0171,0.0164,0.0181,0.0187,0.0194}, {0,0,5.25e-5,7.82e-5,7.78e-5,6.08e-5,5.88e-5}.

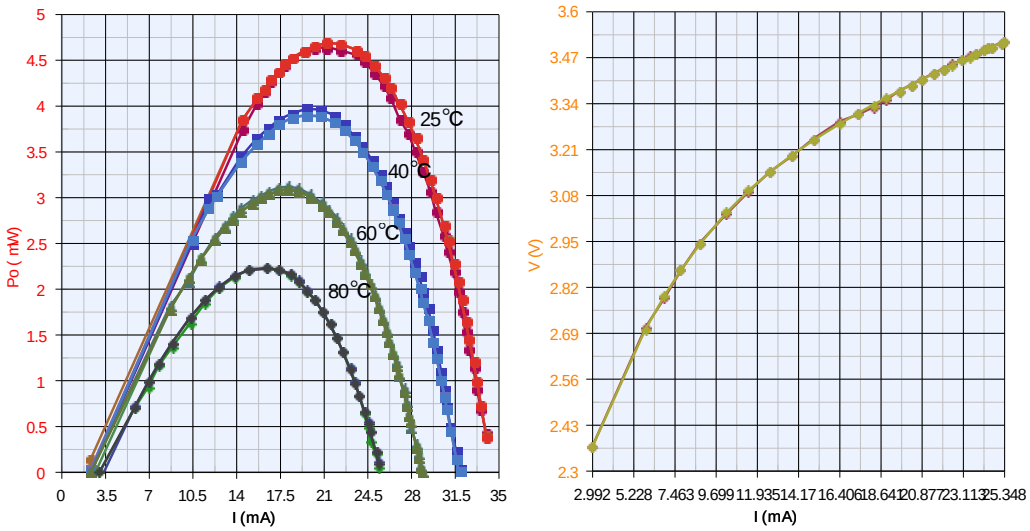

(a) (b)

Figure 2 (a) LI and (b) VI curves of device 1. The curve fits are overlaid on the measurements

The performance of the VCSEL is simulated using the behavior model. Figure 3 shows a comparison of the simulated LI curve with experiment under different ambient temperature conditions.

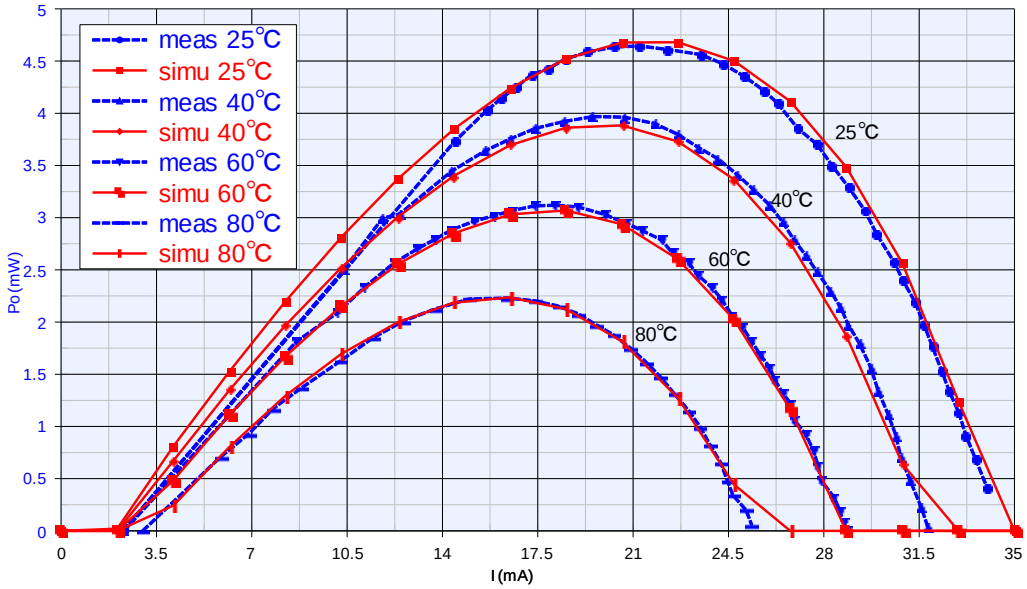

Figure 3 Comparison of measured and simulated LI curves

Device 2

The second device is a 3.1um diameter thin-oxide-aperture VCSEL [10]. The LI, VI and small-signal frequency response of the device are shown in Figure 4. The results of curve fitting result are also shown in Figure 4.

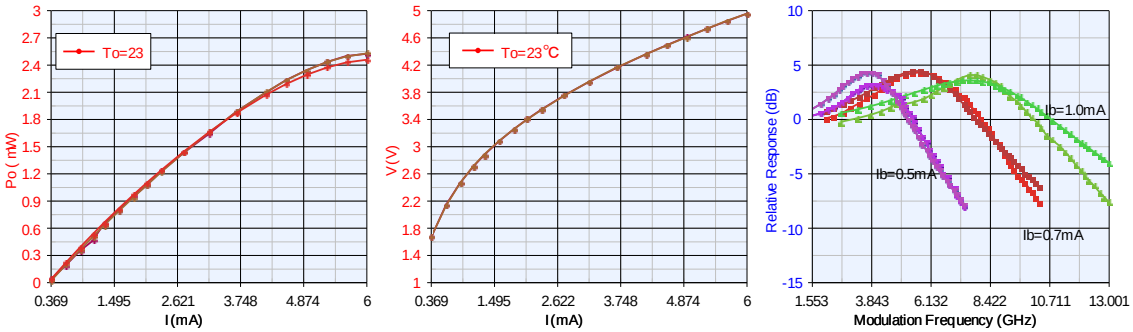

(a) (b) (c)

Figure 4 (a) LI, (b) VI, (c) small-signal frequency response of device 2. The results of curve fitting are overlaid on the measurements.

The extracted behavior for this device yields $\eta = 0.80$ W/A, R_{th} = 1.2 K/mW, I_{tho} = 0.30 mA, $\{a_0, a_1, a_2, a_3, a_4\}$= {–1.33 mA, 6.3e-2 mA/K, –3.5e-4 mA/K^2, 2.6e-6 mA/K^3, 9.7e-8 mA/K^4}, $\eta_i = 1.0$, $\beta = 0.001$, $\tau_n = 0.1$ ns, k = 1.5e-8 W, G_o =8.8e5 s^{-1}, N_o = 4.97e5, $\tau_p = 9$ ps, ε = 0.48e-7. For the VI curve, the coefficients array and the related auxiliary array (α and β) in equation 12 are {3.61 521 –7.8e4 2.1e7 –6.7e9 2.2e12 –7.4e14}, {0 2.9e-3 3.4e-3 3.1e-3 3.2e-3 3.1e-3 3.2e-3}, {0 0 3.2e-6 2.0e-6 2.4e-6 2.1e-6 2.1e-6}. The simulation of the LI characteristics and the small-signal frequency response curve is shown in Figure 5 and Figure 6, respectively.

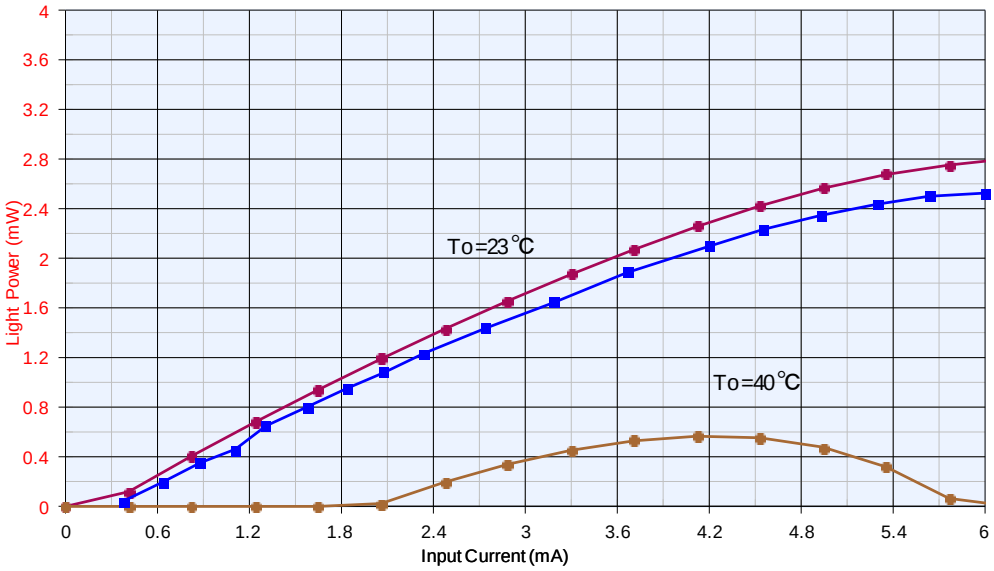

Figure 5 Simulation of LI characteristics for device 2

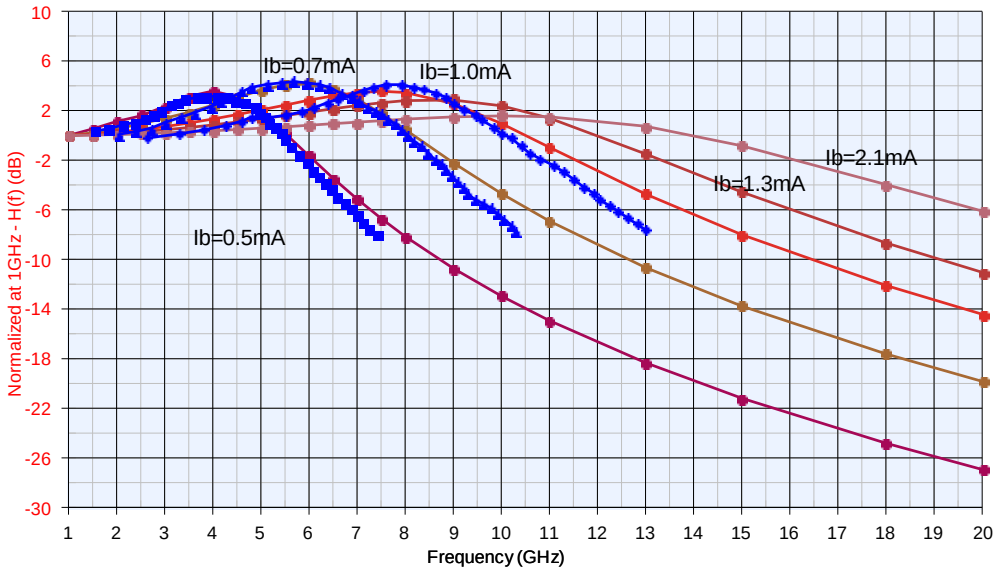

Figure 6 Simulation of the small-signal frequency response for device2. The blue dots are from measurements and the solid lines are simulation.

Device 3

The third device is from [11]. The LI and VI curves are measured at 25°C, along with the frequency response S_{21} curve at bias currents of 3, 6 and 8 mA. The curve fits to the measurements are shown in Figure 7.

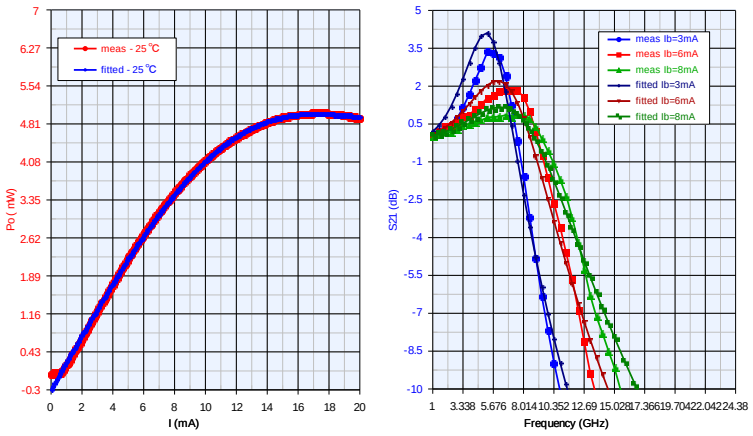

(a) (b)

Figure 7 (a) LI and (b) S21 characteristics of Device 3. The curve fits are overlaid on the experimental data.

The best fit values for the coefficients are η = 0.39 W/A, R_{th} = 4.0 K/mW, I_{tho} = 0.10 mA, $\{a_0, a_1, a_2, a_3, a_4\}$= {2.61mA, -9.40e-2mA/K, 6.53e-4mA/K^2, -0.35e-6mA/K^3, -0.16e-8 mA/K^4}, η_i = 0.69, β =0.001, τ_n =10 ns, k =9.8e-8W, G_o =1.05e6 s^{-1}, N_o =3.81e6, τ_p =1.0 ps, and ε =1.8e-6. The VI curve was fitted using eq.13 by the linear LS method. The coefficients array and the related auxiliary array (α and β) are {2.4 55.6 -2.1e4

1.4e5 -1.1e7 1.3e9 -2.0e11}, {0 0.01 0.01 0.01 0.01 0.01 0.01}, {0 0 3.35e-5 2.68e-5 2.58e-5 2.55e-5 2.54e-5}. Using the extracted values, the performance of the VCSEL is simulated. The results for the LI and the S21 response are shown in Figure 8 and Figure 9, respectively.

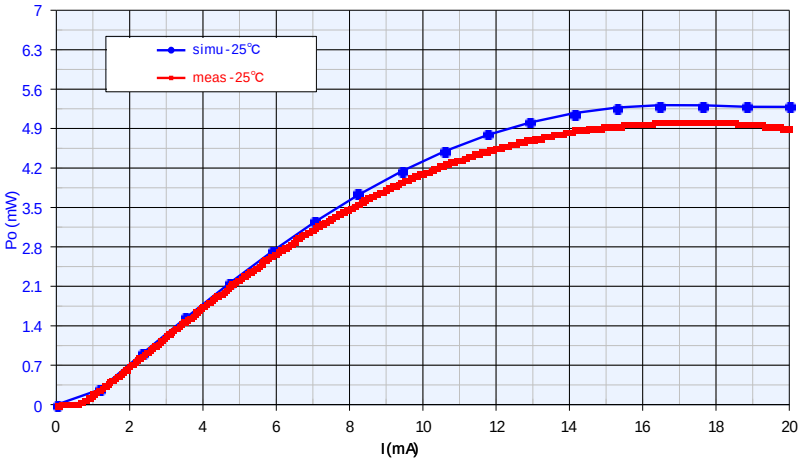

Figure 8 Comparison of simulated with measured LI characteristics of device 3

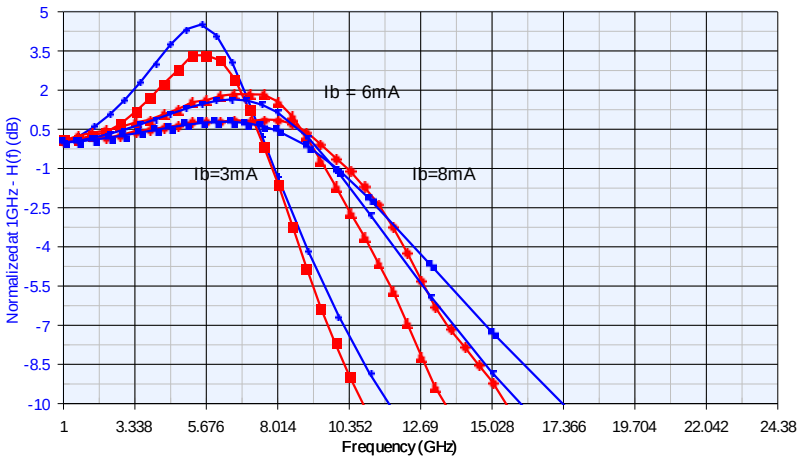

Figure 9 Comparison of simulated and measured small-signal frequency response S21 at several drive currents for device 3

Optical Link Simulation using IBIS-AMI

An entire optical link consisting of electronic and optical components including the VCSEL was setup as shown in Figure 10 and simulated. The electrical data signal is converted to the VCSEL compatible current by the electronic components. The VCSEL converts the electronic signal to an optical signal. After the transmission in the optical medium and conversion back to the electronic signal, the whole optical link is finished. Device 3 was used as the model for the VCSEL to transmit a 10 Gb/s signal. The waveform and eye diagram from the VCSEL are shown in Figure 10 and Figure 11.

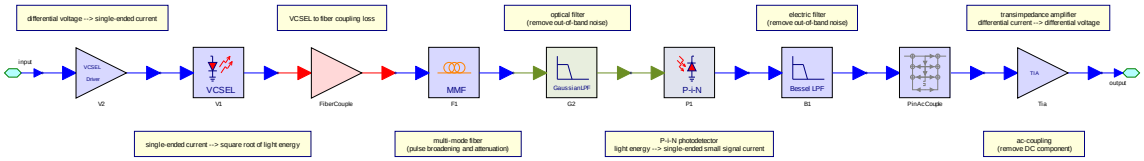

Figure 10 Schematic of optical link simulation

A 10GHz signal transmission is simulated and the waveform and eye diagram can be got as shown in Figure 11.

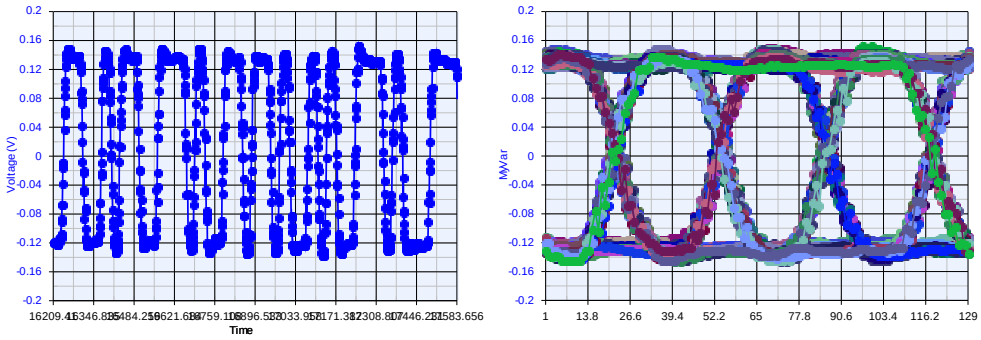

(a) (b)

Figure 11 Simulation of the transmitter with the VCSEL driven at 10 Gb/s. (a) Output optical waveform from the VCSEL driven with a pseudo-random bit sequence and (b) eye diagram.

With the development of the VCSEL model, the entire optical link can be setup and generated in an IBIS-AMI model using EDA tools.

V Conclusions

In this paper, the technique to extract VCSEL devices into IBIS-AMI models has been proposed. A behavior model is generated for the VCSEL using rate equations that incorporate thermal effects. The technique is verified by comparing simulated and measured characteristics of the three different VCSELs. Based on IBIS-AMI, a new way to incorporate optical device into simulation tools is provided.

REFERENCES

[1] Jackson K P, Schow C L, VCSEL-Based Transceivers for Data Communications, Berlin Heidelberg: Springer, 2013, pp. 431-448.

[2] D.M. Kuchta, A. V. Rylyakov, C. L. Schow, J. E. Proesel and C. Baks, "A 55Gb/s Directly Modulated 850nm VCSEL-Based Optical Link," in *IEEE PHOTONICS CONFERENCE 2012*, 2012.

[3] K. Szczerba, P. Westbergh, M. Karlsson, P. A. Andrekson and A. Larsson, "60 Gbits error-free 4-PAM operation with 850nm VCSEL," *ELECTRONICS LETTERS,* vol. 49, no. 15, pp. 953-955, 2013.

[4] Matthias Streiff, ANdreas Witzig, Michael Pfeiffer, Paul Royo and Wolfgang Fichtner, "A Comprehensive VCSEL Device Simulator," *IEEE JOURNAL OF SELECTED TOPICS IN QUANTUM ELECTRONICS,* vol. 9, no. 3, pp. 879-891, 2003.

[5] P. V. Mena, J. J. Morikuni, S. M. Kang, A. V. Harton and K. W. Wyatt, "A Simple Rate-Equation-Based Thermal VCSEL Model," *JOURNAL OF LIGHTWAVE TECHNOLOGY,* vol. 17, no. 5, pp. 865-872, May 1999.

[6] Matt Bruensteiner and George C. Papen, "Extraction of VCSEL Rate-Equation Parameters for Low-Bias System Simulation," *IEEE JOURNAL OF SELECTED TOPICS IN QUANTUM ELECTRONICS,* vol. 5, no. 3, pp. 487-494, 199.

[7] Goldren, L. A. and Corzine, S. W., Diode Lasers and Photonic Integrated Circuits, Chapter 5, New York: Wiley, 1995.

[8] John C. Cartledge and R. C. Srinivasan, "Extraction of DFB Laser Rate Equation Parameters for System Simulation Purposes," *JOURNAL OF LIGHTWAVE TECHNOLOGY,* vol. 15, no. 5, pp. 852-860, 1997.

[9] Y. Ohiso, K. Tateno, Y. Kohama, A. Wakatsuik, H. Tsunetsugu and T. Kurokawa, "Flip-chip bonded 0.85-µm bottom-emitting vertical-cavity laser array on an AlGaAs substrate," *IEEE PHOTON. TECHNOL. LETT.,* vol. 8, pp. 1115-1117, 1996.

[10] B. J. Thibeault, K. Bertilsson, E. R. Hegblom, E. Strzelecka, P. D. Floyd, R. Naone and L. A. Coldren, "High-Speed Characteristics of Low-Optical Loss Oxide-Apertured Vertical-Cavity Lasers," *IEEE PHOTONICS TECHNOLOGY LETTERS,* vol. 9, no. 1, pp. 11-13, 1997.

[11] M. V. Ramana Murty, L. Giovane, S. K. Ray, K. -L. Chew, M. V. Crom, T. E. Sale, A. Sridhara, C. Zhao, Chu Chen and T. R. Fanning, "VCSELs for High-Speed Data Networks," in *Proc. SPIE 8639, Vertical-Cavity Surface-Emitting Lasers XVII, 863902*, 2013.

myKeysight

myKeysight

www.keysight.com/find/mykeysight
A personalized view into the information most relevant to you.

www.axiestandard.org
AdvancedTCA® Extensions for Instrumentation and Test (AXIe) is an open standard that extends the AdvancedTCA for general purpose and semiconductor test. Keysight is a founding member of the AXIe consortium. ATCA®, AdvancedTCA®, and the ATCA logo are registered US trademarks of the PCI Industrial Computer Manufacturers Group.

www.lxistandard.org
LAN eXtensions for Instruments puts the power of Ethernet and the Web inside your test systems. Keysight is a founding member of the LXI consortium.

www.pxisa.org
PCI eXtensions for Instrumentation (PXI) modular instrumentation delivers a rugged, PC-based high-performance measurement and automation system.

Three-Year Warranty
www.keysight.com/find/ThreeYearWarranty
Keysight's commitment to superior product quality and lower total cost of ownership. The only test and measurement company with three-year warranty standard on all instruments, worldwide.

Keysight Assurance Plans
www.keysight.com/find/AssurancePlans
Up to five years of protection and no budgetary surprises to ensure your instruments are operating to specification so you can rely on accurate measurements.

www.keysight.com/quality
Keysight Technologies, Inc.
DEKRA Certified ISO 9001:2008
Quality Management System

Keysight Channel Partners
www.keysight.com/find/channelpartners
Get the best of both worlds: Keysight's measurement expertise and product breadth, combined with channel partner convenience.

For more information on Keysight Technologies' products, applications or services, please contact your local Keysight office. The complete list is available at:
www.keysight.com/find/contactus

Americas

Canada	(877) 894 4414
Brazil	55 11 3351 7010
Mexico	001 800 254 2440
United States	(800) 829 4444

Asia Pacific

Australia	1 800 629 485
China	800 810 0189
Hong Kong	800 938 693
India	1 800 112 929
Japan	0120 (421) 345
Korea	080 769 0800
Malaysia	1 800 888 848
Singapore	1 800 375 8100
Taiwan	0800 047 866
Other AP Countries	(65) 6375 8100

Europe & Middle East

Austria	0800 001122
Belgium	0800 58580
Finland	0800 523252
France	0805 980333
Germany	0800 6270999
Ireland	1800 832700
Israel	1 809 343051
Italy	800 599100
Luxembourg	+32 800 58580
Netherlands	0800 0233200
Russia	8800 5009286
Spain	0800 000154
Sweden	0200 882255
Switzerland	0800 805353 Opt. 1 (DE) Opt. 2 (FR) Opt. 3 (IT)
United Kingdom	0800 0260637

For other unlisted countries:
www.keysight.com/find/contactus
(BP-07-10-14)

KEYSIGHT TECHNOLOGIES

Published in USA, August 4, 2014
5991-4079EN
www.keysight.com